Unusual Metal−Insulator Transitions in the $LaTi_{1-x}V_xO_3$ Perovskite Phases

C. Eylem,[1a,d] Y.-C. Hung,[1a] H. L. Ju,[1b] J. Y. Kim,[1c] D. C. Green,[1a] T. Vogt,[1e] J. A. Hriljac,[1d] B. W. Eichhorn,*[,1a] R. L. Greene,*[,1b] and L. Salamanca-Riba[1c]

Center for Superconductivity Research, Departments of Chemistry, Physics, and Materials Engineering, University of Maryland, College Park, Maryland 20742, and Departments of Applied Science and Physics, Brookhaven National Laboratory, Upton, New York 11973

Received July 28, 1995. Revised Manuscript Received October 18, 1995[⊗]

A series of $LaTi_{1-x}V_xO_3$ compounds ($0 \le x \le 1$) have been prepared by the dc arc-melting method and characterized by conventional powder X-ray diffraction, thermogravimetric analysis, four-probe resistivity, and magnetic susceptibility studies. Selected members of this series have been characterized by synchrotron X-ray diffraction, neutron diffraction, selected area electron diffraction. Samples in the $0.2 \le x \le 0.3$ region are ∼3−4% La deficient (e.g., $La_{0.97}Ti_{0.8}V_{0.2}O_3$). Like the $LaMO_3$ end members where M = Ti, V, the $LaTi_{1-x}V_xO_3$ phases are barely orthorhombic (almost tetragonal) and adopt the perovskite-type $GdFeO_3$ structure (space group *Pnma*). Most of the $LaTi_{1-x}V_xO_3$ phases are antiferromagnetic (AF) insulators including $LaTiO_3$ (T_N = 148 K) and $LaVO_3$ (T_N = 140 K). For the $LaTi_{1-x}V_xO_3$ phases in the $0 < x < 0.10$ region, the AF ordering temperatures and resistivities are reduced with increasing vanadium concentration. The $0.10 \le x \le 0.25$ region comprises poorly metallic ($\rho_{298} \approx 10^{-2}$ Ω cm), paramagnetic phases that represent rare examples of *B*-site-substituted metallic perovskites. Magnetic susceptibility studies in this region show Curie−Weiss behavior below 200 K with large temperature independent susceptibilities of ca. 10^{-3} emu/mol. Variable-temperature synchrotron X-ray diffraction experiments on the $La_{0.97}Ti_{0.8}V_{0.2}O_3$ phase showed a marked orthorhombic distortion below 150 K but a nearly tetragonal cell at 298 K. Rietveld refinements of neutron diffraction data for this phase at 50 K showed a prototypical $GdFeO_3$ structure with disordered Ti and V (refined occupancies of 82(1)% and 18(1)%, respectively) distributed over the octahedral site and a slight La deficiency (refined occupancy = 97(1)%). The structural parameters (bond distances, angles, cell constants) are intermediate to those of the $LaMO_3$ end members as expected. Electron diffraction experiments on the $La_{0.97}Ti_{0.8}V_{0.2}O_3$ phase revealed diffraction patterns that were also consistent with the prototypical *Pnma* cell with no evidence of microdomain ordering or supercell formation. In the $0.25 < x \le 1.0$ region, the samples again show AF ordering and insulating behavior. The magnetic susceptibilities of the samples in this region show unusual peaking that is compositionally dependent. The field-cooled magnetic susceptibility of the $x = 0.90$ and 1.0 samples show large diamagnetic signals of unexplained origin. The zero-field cooled susceptibilities of these samples showed paramagnetic behavior. The formation of metallic phases from *B*-site substitution is discussed in terms of the Hubbard model.

Introduction

The study of metal−insulator (M−I) transitions in transition-metal oxide systems is of current interest to the solid-state chemistry and physics communities.[2−4] Recent theories have been advanced that classify most binary and simple ternary insulating oxides arising from M−I instabilities into two distinct categories; namely Mott−Hubbard (M−H) and charge-transfer (C−T) insulators.[5] In a Zaanen−Sawatzky−Allen (ZSA) formalism, one differentiates between M−H and C−T insulators according to the nature of the lowest energy band gap in the compound.[6] In a M−H insulator, the lowest energy gap is between upper and lower Hubbard bands. Both Hubbard bands are transition-metal-based d states that arise from electron−electron correlations. An equivalent description using the Goodenough model[7,8] attributes the gap in a Mott−Hubbard insulator to valence fluctuation or charge disproportionation of the transition metal ions; e.g., $d^n + d^n \rightarrow d^{n+1} + d^{n-1}$. The energy of this process is defined as the electron correlation energy, *U* (the "Hubbard" *U*). In a charge-transfer insulator, the lowest energy gap is between a filled oxygen state and an empty metal-based state. In general, early-transition-metal oxides can be broadly

⊗ Abstract published in *Advance ACS Abstracts*, December 1, 1995.

(1) (a) Maryland, Chemistry. (b) Maryland, Physics. (c) Maryland, Materials Engineering. (d) Brookhaven, Applied Science. (e) Brookhaven, Physics.

(2) Mott, N. *Metal-Insulator Transitions*, 2nd ed.; Taylor and Francis: New York, 1990.

(3) Torrance, J. B.; Lacorre, P.; Asavaroengchai, C.; Metzger, R. M. *Physica C* **1991**, *182*, 351.

(4) Burdett, J. K. *Chemical Bonding in Solids*; Oxford University Press: New York, 1995; p 144.

(5) Torrance, J. B.; Lacorre, P.; Asavaroengchai, C.; Metzger, R. M. *J. Solid State Chem.* **1991**, *90*, 168.

(6) Zaanen, J.; Sawatzky, G. A.; Allen, J. W. *Phys. Rev. Lett.* **1985**, *55*, 418.

(7) Goodenough, J. B.; Longo, J. M. In *Landolt-Bornstein*; Springer-Verlag: Berlin, 1970; Vol. Group III/4a, p 129.

(8) Goodenough, J. B. *Prog. Solid State Chem.* **1975**, *5*, 145.

0897-4756/96/2808-0418$12.00/0

classified as Mott−Hubbard type insulators (except d^0 compounds) whereas late-transition-metal oxides are of the charge-transfer type.

In substituted systems with variable compositions (e.g., solid solutions, oxygen defects, etc.), experimental differentiation of the various localization modes that cause M−I transitions is difficult and more than one source of localization may be important near an M−I boundary (e.g., impurity states, magnetic ordering, etc.). Several theories have been advanced that describe different phenomena leading to electron localization. In an Anderson type transition, localization arises from local aperiodic perturbations of the crystal potential due to nonuniform populations of lattice sites in the crystal.[9] Thus M−I transitions occurring in solid solutions, such as the $Sr_{1-x}R_xVO_3$ phases ($d^1 \rightarrow d^2$) where R = rare earth, are often attributed to Anderson type transitions[10,11] due to the large differences in potential between Sr^{2+} and R^{3+}.

Other compounds, such as the $R_{1-x}A_xTiO_3$ phases ($d^1 \rightarrow d^0$) where A = alkaline earth and R = rare earth, undergo M−I transitions that are supposedly of the Mott−Hubbard type.[12−18] The M−I transitions are often related to changes in structural parameters, such as an M−O distance or an M−O−M angle. These structural parameters control the bandwidths (W) of the Hubbard bands thus directly affecting the U/W ratio and ultimately the transport properties. According to Mott−Hubbard theory, an insulating state is obtained when $U/W > 1$ and metallic behavior is observed when $U/W < 1$. For example, the $R_{1-x}A_xTiO_3$ phases ($d^1 \rightarrow d^0$) generally display metallic behavior when $\sim 0.1 < x < \sim 0.9$ ($U/W < 1$); however, a bandgap opens as one approaches the d^1 configuration ($U/W > 1$) due to electron−electron correlation (i.e., a correlation gap). As a result, the partially filled one-electron d band splits into a filled lower Hubbard band and an empty upper Hubbard band giving rise to an AF insulating state. Recent reinvestigations of the $R_{1-x}Sr_xVO_3$ compounds indicate that the M−I transitions are also of the Mott−Hubbard type[19] and not Anderson localizations as originally suggested.[10,11]

We are interested in studying the origins of M−I transitions in early transition metal perovskites. In particular, we have investigated the electronic structures of various "hole-doped" d^1 titanate perovskites (i.e., $d^1 \rightarrow d^0$) of composition $R_{1-x}A_xTiO_3$ where A = alkaline earth and R = rare earth.[12,13,18,20−22] This class of compounds shows two M−I transition boundaries; one at high carrier concentration (close to d^1) and one at low carrier concentration (close to d^0). Analysis of the structural, transport, and magnetic data shows that both series of M−I transitions are closely related to the structural and magnetic properties and can be broadly classified as Mott−Hubbard types. Photoemission studies support these findings and show Fermi liquidlike behavior as the M−I transition close to the d^1 configuration is approached.[20,22] In an attempt to disrupt antiferromagnetic ordering in $LaTiO_3$ by way of "electron doping" (i.e., $d^1 \rightarrow d^2$), we have prepared solid solutions of the known antiferromagnetic (AF) insulators $LaTiO_3$ (Ti^{3+}, d^1)[23−25] and $LaVO_3$ (V^{3+}, d^2).[10,26−28] Above 100 K, both compounds adopt distorted perovskite structures (the $GdFeO_3$ structure type) as shown in Figure 1. In this paper, we describe an unusual M−I transition in the $LaTi_{1-x}V_xO_3$ series where a narrow metallic region is formed. This system seems to be an ideal candidate for an Anderson type instability and sustained insulating behavior because the substitution involves the elements whose orbitals define the upper and lower Hubbard bands and large aperiodic perturbations of the crystal potential at the Fermi surface would be expected. However, the antiferromagnetic ordering is disrupted and metallic-like conductivity is observed in the range $0.10 \leq x \leq 0.25$.

Experimental Section

Sample Preparation. Solid solutions of $LaTi_{1-x}V_xO_3$ ($0 \leq x \leq 1$) were prepared by arc-melting pelletized mixtures of predried La_2O_3 (99.99%), V_2O_3 (99.9%), TiO_2 (99.5%), and Ti (99.5%). The phases where $x \leq 0.25$ were also prepared from La_2O_3, TiO_2, Ti, and V metal. The oxygen contents of the precursors were adjusted to be 1% oxygen deficient (i.e., $LaTi_{1-x}V_xO_{2.97}$) to compensate for the slight oxidation in the arc furnace. The pelletized mixtures and a button of zirconium metal were placed in separate cavities of a water-cooled copper hearth inside an arc furnace that was evacuated and purged with gettered Ar (UHP) gas several times before the reaction. Before each pellet was fired, the Zr metal was melted in order to purify the atmosphere inside the furnace. Samples were fired several times with repetitive turnings. The resulting phases were then pulverized in percussion mortar, finely ground, and analyzed by powder X-ray diffraction (XRD). Each sample was prepared and characterized at least twice. The syntheses were highly reproducible. All single-phase samples were stored in a Vacuum Atmospheres drybox to prevent oxidation.

Sample Characterization. *Powder X-ray Diffraction.* X-ray diffraction (XRD) data were collected at 25 °C on a Rigaku θ-θ D/MAX-B diffractometer (Cu Kα radiation) and processed using an MDI Software System. Cell refinement calculations were performed on all data collected between $20° < 2\theta < 80°$ and were corrected for sample displacement and zero-point error.

(9) Anderson, P. W. *Phys. Rev.* **1958**, *109*, 1492.
(10) Dougier, P.; Hagenmuller, P. *J. Solid State Chem.* **1975**, *15*, 158.
(11) Mott, N. F.; Pepper, M.; Pollitt, S.; Wallis, R. H.; Adkins, C. J. *Proc. R. Soc. London, Ser A* **1975**, *345*, 169.
(12) Eylem, C.; Sághi-Szabó, G.; Chen, B.-H.; Eichhorn, B.; Peng, J.-L.; Greene, R.; Salamanca-Riba, L.; Nahm, S. *Chem. Mater.* **1992**, *4*, 1038.
(13) Eylem, C.; Eichhorn, B. W.; Ju, H. L.; Greene, R. *J. Solid State Chem.* **1995**, *114*, 164.
(14) Sunstrom, J. E.; Kauzlarich, S. M.; Klavins, P. *Chem. Mater.* **1992**, *4*, 346.
(15) Sunstrom, J. E.; Kauzlarich, S. M. *Chem. Mater.* **1993**, *5*, 1539.
(16) Taguchi, Y.; Tokura, Y.; Arima, T.; Inaba, F. *Phys. Rev. B* **1993**, *48*, 511.
(17) Tokura, Y.; Taguchi, Y.; Okada, Y.; Fujishima, Y.; Arima, T.; Kumangi, K.; Iye, Y. *Phys. Rev. Lett.* **1993**, *70*, 2126.
(18) Ju, H. L.; Eylem, C.; Eichhorn, B. W.; Greene, R. L. *Phys. Rev. B* **1994**, *49*, 13335.
(19) Mahajan, A. V.; Johnston, D. C.; Torgeson, D. R.; Borsa, F. *Phys. Rev. B* **1992**, *46*, 10973.
(20) Robey, S. W.; Hudson, L. T.; Eylem, C.; Eichhorn, B. W. *Phys. Rev. B* **1993**, *48*, 562.
(21) Robey, S. W.; Hudson, L. T.; Eylem, C.; Eichhorn, B. W. *J. Superconduct.* **1995**, *7*, 917.
(22) Robey, S. W.; Henrich, V. E.; Eylem, C.; Eichhorn, B. W. *Phys. Rev. B* **1995**, *52*, 2395.
(23) Lichtenberg, F.; Widmer, D.; Bednorz, J. G.; Williams, T.; Reller, A. *Z. Phys. B* **1991**, *82*, 211.
(24) MacEachern, M. J.; Dabkowska, H.; Garrett, J. D.; Amow, G.; Gong, W.; Liu, G.; Greedan, J. E. *Chem. Mater.* **1994**, *6*, 2092.
(25) Crandles, D. A.; Timusk, T.; Garrett, J. D.; Greedan, J. E. *Phys. Rev. B* **1994**, *49*, 16207.
(26) Rogers, D. B.; Ferretti, A.; Ridgley, D. H.; Arnott, R. J.; Goodenough, J. B. *J. Appl. Phys.* **1966**, *37*, 1431.
(27) Dougier, P.; Hagenmuller, P. *J. Solid State Chem.* **1974**, *11*, 177.
(28) Mahajan, A. V.; Johnston, D. C.; Torgeson, D. R.; Borsa, F. *Phys. Rev. B* **1992**, *46*, 10966.

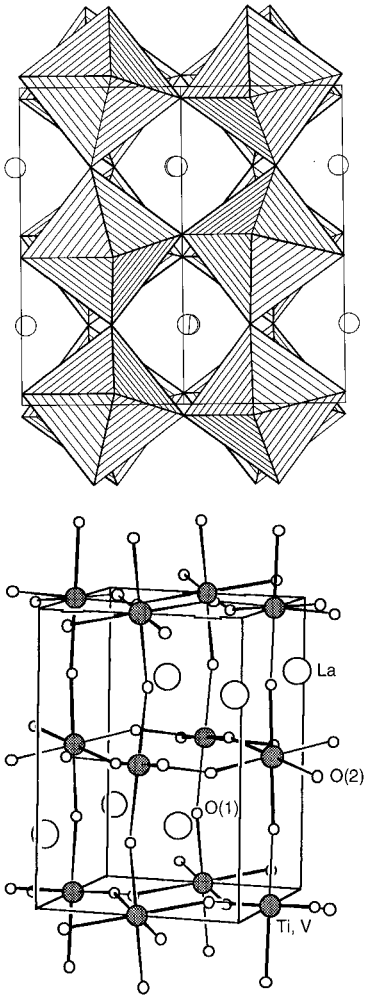

Figure 1. (a, top) Polyhedral representation of the $GdFeO_3$ structure of the $LaMO_3$ phases (M = Ti, V) showing the $MO_{6/2}$ octhedra and La^{3+} ions (spheres). (b, bottom) Ball-and-stick representation of the same structure showing the atomic numbering scheme used in the text and Tables 2 and 3.

Synchrotron X-ray Diffraction. The synchrotron X-ray data were collected on flat-plate samples using the high-resolution mode[29] with a crystal analyzer at the X7A beamline of the National Synchrotron Light Source (NSLS), Brookhaven National Laboratory. A complete ($5° < 2\theta < 40°$) data set was collected at room temperature at a wavelength of 0.7006 Å using a Ge(111)/Ge(222) monochromator/analyzer combination. In a second experiment, the variation in two selected angular regions, ca. 35.5−36.6° and 41.3−41.9° in 2θ, were followed from room temperature to 17 K using a Displex cryogenic unit with a Be window. More extensive X-ray data were collected at 17 K from 5° to 25° in 2θ with a step size of 0.004°. The latter experiments were performed at a wavelength of 0.6988 Å using a Ge(111)/Ge(222) monochromator/analyzer combination. The wavelengths used for the experiments were obtained by calibration with a reference sample of Si powder.

Neutron Diffraction. The high-resolution powder neutron diffraction data were obtained at beamline H1A at the High Flux Beam Reactor (HFBR) at Brookhaven National Laboratory. The sample consisted of ca. 10 g of powder contained in a vanadium can sealed with indium to prevent exposure to the atmosphere. The data were collected at 50 K with a wavelength of 1.8857 Å using 11′ primary collimation and 5′ collimation in front of each of the 64 ^3He detectors. A step size of 0.05° was used in the range of 5−157° in 2θ.

The data were analyzed by the Rietveld method[30] using the GSAS program of Larson and Von Dreele.[31] The background was defined by a series of points connected by linear interpolations and was fixed during refinements. Initial structural analysis involved the refinements of the lattice parameters and zero-point and the Gaussian terms. Structural parameters were then added and refined to reasonable values. Subsequently, temperature factors and Lorentzian terms were refined simultaneously. In the next cycle, Ti/V fractions were constrained (summed occupancy equals 1) and refined together with temperature factors. Finally, the La and O occupancies were refined independently.

Electron Diffraction. Electron diffraction (ED) and high-resolution transmission electron microscopic (HREM) studies were conducted on a JEOL 2000-FXII transmission electron microscope operated at 200 kV. The microscope specifications are spherical aberration coefficient $C_s = 2.3$ mm, chromatic aberration coefficient $C_c = 2.2$ mm, lattice resolution of 0.14 nm, and point image resolution of 0.28 nm. All lattice images were obtained using axial illumination. The samples for HREM studies were prepared from freshly synthesized $LaTi_{1-x}V_xO_3$ materials which were cut with a knife to obtain a fresh surface. During this process, several small crystals were obtained from the new surface and were placed between two copper folding grids for HREM observation.

Compositional Analysis. Oxygen contents were determined by thermogravimetric analysis (TGA). Large samples (∼200 mg) were loaded into platinum boats and heated in air at 900 °C for 12 h, resulting in light yellow powders. The oxygen contents were calculated from the weight gains upon oxidation. XRD analysis of the oxidized samples showed stoichiometric amounts of $La_2Ti_2O_7$ and $LaVO_4$. It was therefore assumed that the final oxidation states of Ti and V in the oxidized samples were +4 and +5, respectively. The uncertainty of the measurements was checked with a reference oxidation process where Ti metal was oxidized to TiO_2. The expected oxygen uptake was determined with a ≤1% error.

The homogeneity of the samples in the composition region $0.1 \le x < 0.3$ was studied by energy-dispersive X-ray analysis (EDX) using a JEOL Model 840 JXA analyzer. EDX analysis of the $x = 0.20$ phase was also monitored in the transmission electron microscope.

Property Measurements. Magnetic susceptibilities of the $LaTi_{1-x}V_xO_3$ compounds were measured from arc melted pellets that were suspended by dental floss in a Quantum Design SQUID magnetometer at an applied field of 1 kG. Remnant moment experiments were conducted by cooling the samples from room temperature to 4 K in a 35 kG field, adjusting to zero field, and measuring the remnant magnetization.

Resistivity measurements were made by using a standard four-probe technique. Arc melted $LaTi_{1-x}V_xO_3$ samples were cut with a diamond saw into rectangular blocks, typically 1.5 × 0.4 × 0.2 mm^3, and polished. Care was taken to avoid pieces containing cracks. Au wires were attached to the samples with silver paste. At least two measurements were made on each composition using samples from different preparations. The data obtained from the different preparations were identical within experimental error. Resistance was measured by cooling the samples from room temperature to 4 K and again upon warming to room temperature to test for hysteresis.

Results

Synthesis and Structure. Ten $LaTi_{1-x}V_xO_3$ samples where $0 \le x \le 1$ were prepared by the dc arc melting technique. The oxygen contents of the $LaTi_{1-x}V_xO_3$ compounds were closely monitored and found to be 3.03 (±0.02). A 1% oxygen deficiency in the starting mixtures was necessary to obtain single-phase samples. Samples for the $x = 0.20$ and 0.25 compounds were slightly La-deficient, having the compositions $La_{0.97}$-

(29) Cox, D. E.; Toby, B. H.; Eddy, M. M. *Aust. J. Phys.* **1988**, *41*, 117.
(30) Rietveld, H. M. *J. Appl. Crystallogr.* **1969**, *2*, 65.
(31) Larson, A. C.; Von Dreele, R. B. GSAS: General Structure Analysis System; Los Alamos National Laboratory, Los Alamos, NM, 1994.

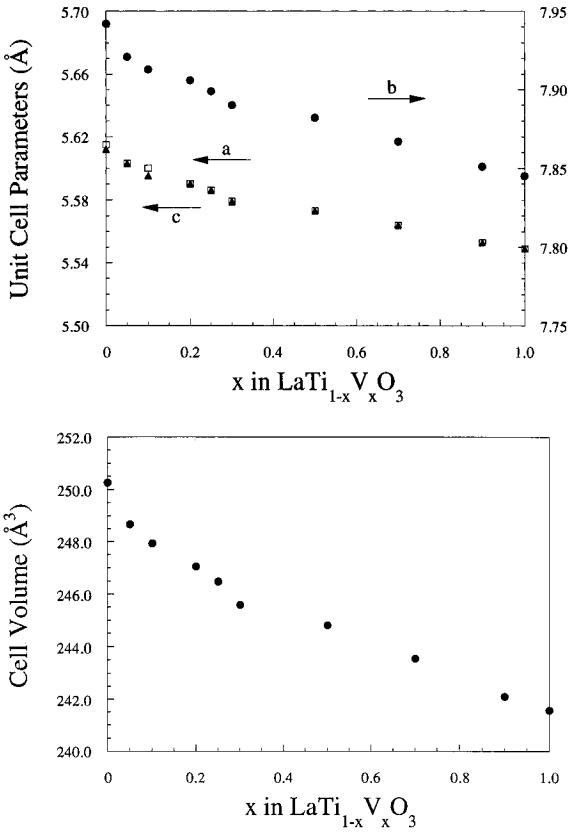

Figure 2. (a, top) Unit-cell parameters for $LaTi_{1-x}V_xO_3$ phases from XRD refinements. All data were indexed in orthorhombic symmetry, but beyond $x = 0.2$, the *a* and *c* cell parameters were indistinguishable. (b, bottom) Plot of cell volume (orthorhombic) versus *x* for the $LaTi_{1-x}V_xO_3$ phases.

$Ti_{0.80}V_{0.20}O_{3.02}$ and $La_{0.97}Ti_{0.75}V_{0.25}O_{3.04}$, respectively. Samples in this range that were prepared from compositions stoichiometric in La contained an unidentified impurity in the XRD profiles. Compositions with larger La deficiencies resulted in heterogeneous samples containing $LaVO_4$ and LaV/Ti/O perovskites.

EDX analyses were performed on representative samples within the metallic region (see below) where $0.10 \leq x \leq 0.25$ to check for sample homogeneity. Analysis of several individual crystallites showed invariant distributions of La, V, and Ti from grain to grain within a given sample.

Attempts to introduce extra oxygen into the $LaTi_{1-x}V_xO_3$ phases (i.e., $LaTi_{1-x}V_xO_{3+\delta}$ phases) were unsuccessful, resulting in mixtures of La/Ti/V/O perovskites, $LaVO_4$ (V^{5+}, d^0), La_2O_3, and other unidentified impurities. The stability of the $LaVO_{3+\delta}$ compounds were also investigated, and, unlike the $LaTiO_{3+\delta}$ phases,[23−25] compositions of formula $LaVO_{3+\delta}$ disproportionated to the $LaVO_3$ (V^{3+}, d^2) and $LaVO_4$ (V^{5+}, d^0) when arc melted or heated in sealed silica tubes at ~1100 °C for 2 days.

The XRD data for all $LaTi_{1-x}V_xO_3$ samples were indexed on an orthorhombic cell corresponding to a $GdFeO_3$ perovskite type structure where $a \approx c \approx \sqrt{2}a_p$, $b \approx 2a_p$ (a_p is the primitive cubic unit-cell constant of a prototypical perovskite, ~3.9 Å). The changes in unit cell parameters and cell volume vary uniformly as a function of *x* and are shown in Figure 2a,b, respectively. The cell parameters, TGA, magnetic and transport data for the $LaTi_{1-x}V_xO_3$ compounds are summarized in Table 1. An XRD profile of the $x = 0.20$ phase is shown in Figure 3 as an example.

As expected, substitution of smaller V^{3+} ion ($r = 0.780$ Å) for the larger Ti^{3+} ion ($r = 0.81$ Å)[32] results in the slight decrease of the cell volume. Although the $LaTi_{1-x}V_xO_3$ samples were indexed on orthorhombic cells for comparison, the *a* and *c* unit cell parameters are indistinguishable by XRD in the $0.2 \leq x < 1.0$ region, and the data can be refined equally well under tetragonal symmetry.

In an attempt to determine the correct crystal system for the $La_{0.97}Ti_{0.8}V_{0.2}O_3$ phase (i.e., tetragonal or orthorhombic), a variable-temperature synchrotron X-ray diffraction (SXRD) study was performed. The room-temperature SXRD profiles are quite similar to the XRD data (Figure 3) and can also be indexed on a tetragonal cell. However, the low-temperature SXRD data ($T \leq 150$ K) clearly reveal a $GdFeO_3$ type orthorhombic cell with absences consistent with the prototypical *Pnma* space group. The lattice constants, which were calculated from the (080), (440), and (044) reflections, are plotted as a function of temperature in Figure 4. The degree of orthorhombicity increases with a slight decrease in overall cell volume as the temperature is lowered. It is interesting to note that the decrease in *a* is not as pronounced as the decrease in *c*. Although the SXRD profiles appear tetragonal at room temperature, we believe that the structure of $La_{0.97}Ti_{0.8}V_{0.2}O_3$ is barely orthorhombic at all temperatures studied (17 K $\leq T \leq$ 298 K) and lower symmetry monoclinic cells are not involved. These conclusions are based on the following analyses of the SXRD data.

Starting from a simple cubic perovskite ($a_p \approx 3.9$ Å), the cubic (222) reflection becomes (044) when the symmetry is tetragonal ($a = c \approx \sqrt{2}a_p$, $b \approx 2a_p$) and this reflection splits into (440) and (044) when the symmetry is further lowered to orthorhombic ($a \approx \sqrt{2}a_p$, $b \approx 2a_p$, $c \approx \sqrt{2}a_p$). Similarly, the cubic (3 $^3/_2$ 1) reflection transforms to (234) in tetragonal and (234) and (432) in orthorhombic symmetry. However, the cubic (400) reflection splits into (404) and (080) when the symmetry is either tetragonal or orthorhombic. Thus, monitoring the cubic (222), (3 $^3/_2$ 1), and (400) reflections of $La_{0.97}Ti_{0.8}V_{0.2}O_3$ is sufficient to determine the crystal symmetry at various temperatures. Additional splitting would be observed for a further reduction in crystal symmetry to monoclinic. The cubic (400) reflection is split into two reflections, the (404) and (080), throughout the temperature range being studied, suggesting that the true symmetry could be either tetragonal or orthorhombic. We did not see any further splitting suggestive of lower symmetry. As shown in Figure 5, the full width at half-maximum (fwhm) of the (404) and (080) reflections are essentially constant from room temperature to 17 K. In contrast, the fwhm of the "tetragonal (044)" broadens with decreasing temperature (Figure 5) and splits into two peaks below 150 K (Figure 6) signifying orthorhombic symmetry in this region. The absence of clear splitting of this peak and the (3 $^3/_2$ 1) cubic reflection at room temperature suggests that the symmetry could be either tetragonal or barely orthorhombic. Refined room-temperature cell parameters for this phase, obtained from a full pattern

(32) Shannon, R. D. *Acta Crystallogr.* **1976**, *A32*, 751.

Table 1. Summary of the Structural Parameters and Magnetic and Transport Properties of the $LaTi_{1-x}V_xO_{3+\delta}$ Phases

compound	*a*	*b*	*c*	volume	oxygen[a] content	transport[b] properties	magnetic[c] properties
$LaTiO_3$	5.615(3)	7.942(4)	5.612(3)	250.26	3.01	SC	AF
$LaTi_{0.95}V_{0.05}O_3$	5.603(2)	7.921(3)	5.603(2)	248.67	3.03	SC	AF
$LaTi_{0.9}V_{0.1}O_3$	5.600(6)	7.913(7)	5.595(5)	247.93	3.02	M	PP
$La_{0.97}Ti_{0.8}V_{0.2}O_3$	5.590(2)	7.906(2)	5.590(2)	247.05	3.02	M	PP
$La_{0.97}Ti_{0.75}V_{0.25}O_3$	5.586(3)	7.899(4)	5.586(3)	246.48	3.04	M−SC	PP
$LaTi_{0.7}V_{0.3}O_3$	5.579(2)	7.890(2)	5.579(2)	245.58	3.03	SC	AF
$LaTi_{0.5}V_{0.5}O_3$	5.573(2)	7.882(3)	5.573(2)	244.80	3.05	SC	AF
$LaTi_{0.3}V_{0.7}O_3$	5.564(2)	7.867(2)	5.564(2)	243.55	3.05	SC	AF
$LaTi_{0.1}V_{0.9}O_3$	5.553(3)	7.851(3)	5.553(3)	242.09	3.03	SC	AF
$LaVO_3$	5.549(2)	7.845(1)	5.549(2)	241.56	3.02	SC	AF

[a] Errors are ±0.02. [b] SC = semiconductor; M = metallic. [c] AF = antiferromagnetic; PP = Pauli paramagnetic.

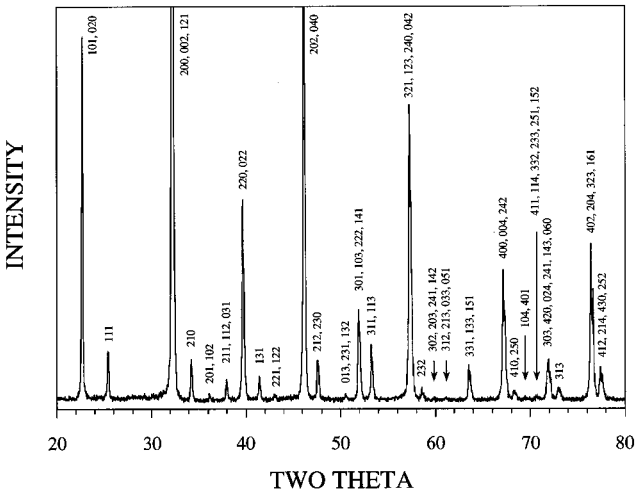

Figure 3. Indexed conventional X-ray diffraction profile for $La_{0.97}Ti_{0.8}V_{0.2}O_3$.

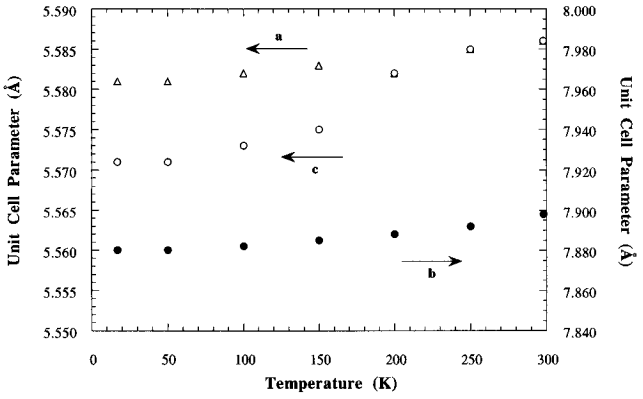

Figure 4. Unit-cell parameters of $La_{0.97}Ti_{0.8}V_{0.2}O_3$ as a function of temperature as determined from variable-temperature synchrotron X-ray diffraction.

decomposition using the method described by Le Bail et al.,[33] indicate a barely orthorhombic cell with lattice parameters, $a = 5.5868(2)$, $b = 7.8927(2)$, $c = 5.5861(2)$. The broadening of the "tetragonal (044)" is also consistent with an orthorhombic cell in this region. Moreover, the absences of anomalies in the cell volumes, transport properties, or magnetic properties between 17 and 298 K suggests that structural phase transition is not occurring in this temperature region. Similar variations in the orthorhombic region of $LaVO_3$ (100 → 298 K) were reported by Bordet et al.[34]

Note that $La_{0.97}Ti_{0.8}V_{0.2}O_3$ contains a small amount of an impurity phase that appears as shoulders on the high-angle reflections (see Figure 6). These shoulders were not evident in the XRD profiles (Figure 3).

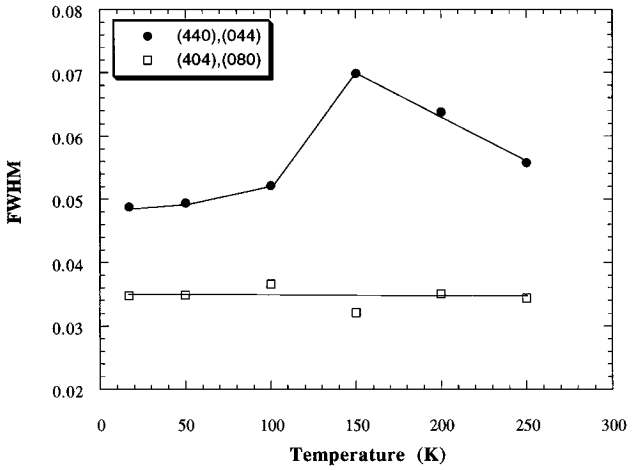

Figure 5. Plot of full width at half-maximum (fwhm) of the (440),(044) and (404),(080) reflection pairs (synchrotron X-ray diffraction) versus temperature. The (440) and (044) reflections were fit as one peak between 150 and 250 K and as two peaks below 150 K. The (404) and (080) reflections were fit as two individual peaks throughout the temperature range being studied.

Because of the unusual magnetic and transport behavior of the $La_{0.97}Ti_{0.8}V_{0.2}O_3$ phase, electron diffraction (ED) studies were initiated to probe for superstructure formation and/or microdomain ordering. ED data were collected on several crystallites of several different $La_{0.97}Ti_{0.8}V_{0.2}O_3$ samples, and three representative diffraction patterns are shown in Figure 7. Multiple zone axes of each crystallite were examined to check for extraneous peaks due to multiple diffraction, consistency in the cell constants, and trends of reflection conditions. The diffraction patterns were highly reproducible and were indicative of a 5.6 × 7.9 × 5.6 Å cell, which is in excellent agreement with the refinements of the XRD and synchrotron data. Like the X-ray experiments, we were unable to distinguish between tetragonal and orthorhombic cells (or differentiate *a* or *c* cell axes) in the ED experiments. Despite the prevalent double diffraction peaks (e.g., Figure 7a,b) and ambiguities in cell axes, the extinction conditions were clearly indicative of orthorhombic space group *Pnma* (Figure 7c,d).

The inability to distinguish Ti from V and problems associated with determining oxygen positions limited

(33) A modified version of the Rietveld program: Le Bail, A.; Duroy, H.; Fourquet, J. L. *Mater. Res. Bull.* **1988**, *23*, 447.

(34) Bordet, P.; Chaillout, C.; Marezio, M.; Huang, Q.; Santoro, A.; Cheong, S.-W.; Takagi, H.; Oglesby, C. S.; Batlogg, B. *J. Solid State Chem.* **1993**, *106*, 253.

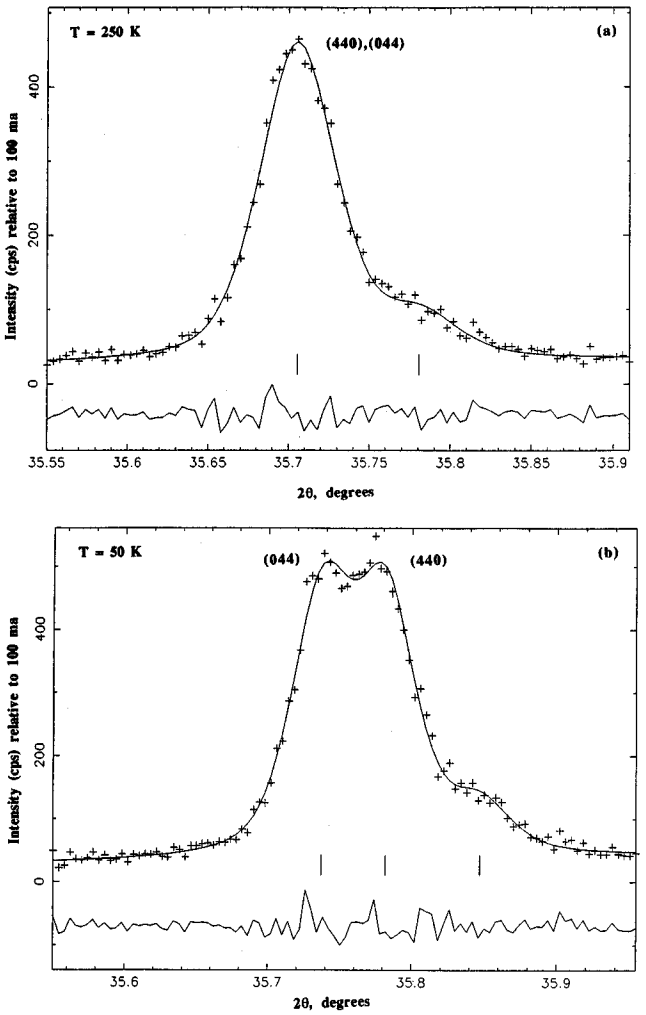

Figure 6. Least-squares profile fits for the orthorhombic (440),(044) reflections (synchrotron X-ray diffraction) at (a) 250 and (b) 50 K. The peak at higher angle belongs to an impurity phase.

the amount of structural information attainable from the SXRD and XRD studies. To circumvent these problems, low-temperature neutron diffraction studies were carried out on the $La_{0.97}Ti_{0.8}V_{0.2}O_3$ phase. Careful inspection of the neutron data revealed absences of reflections with $0kl$, $k+l \neq 2n$; $hk0$, $h \neq 2n$; $h00$, $h \neq 2n$; $0k0$, $k \neq 2n$; $00l$, $l \neq 2n$, consistent with space group *Pnma*. The starting model for the Rietveld refinement, therefore, consisted of the atomic positions obtained from orthorhombic $LaTiO_3$ structure.[35] Plots of calculated and observed neutron diffraction profiles are shown in Figure 8, and a summary of the refined parameters is given in Table 2. Selected interatomic distances, angles the cell parameters for $La_{0.97}Ti_{0.8}V_{0.2}O_3$ and the $LaMO_3$ end members are given in Table 3. The reliability factors are slightly high due to weak shoulders that do not appear to belong to the main orthorhombic phase.

The refined occupancies from the neutron diffraction study of $La_{0.97}Ti_{0.8}V_{0.2}O_3$ gave the following results: La, 0.97(1); Ti, 0.82(1); V, 0.18(1); O, 3.07(5). These data along with the continuous change in cell parameters and distances and angles indicate that the $La_{0.97}Ti_{0.8}V_{0.2}O_3$ phase is a typical $GdFeO_3$-type structure with Ti and V statistically disordered over the octahedral (4b) site. The M−O distances and cell parameters decrease as the M−O−M angles increase with increasing x as expected. Somewhat surprisingly, the structural parameters of $La_{0.97}Ti_{0.8}V_{0.2}O_3$ more closely resemble those of $LaVO_3$ rather than $LaTiO_3$ (Table 3). The M−O distances and M−O−M angles directly affect the band widths of the

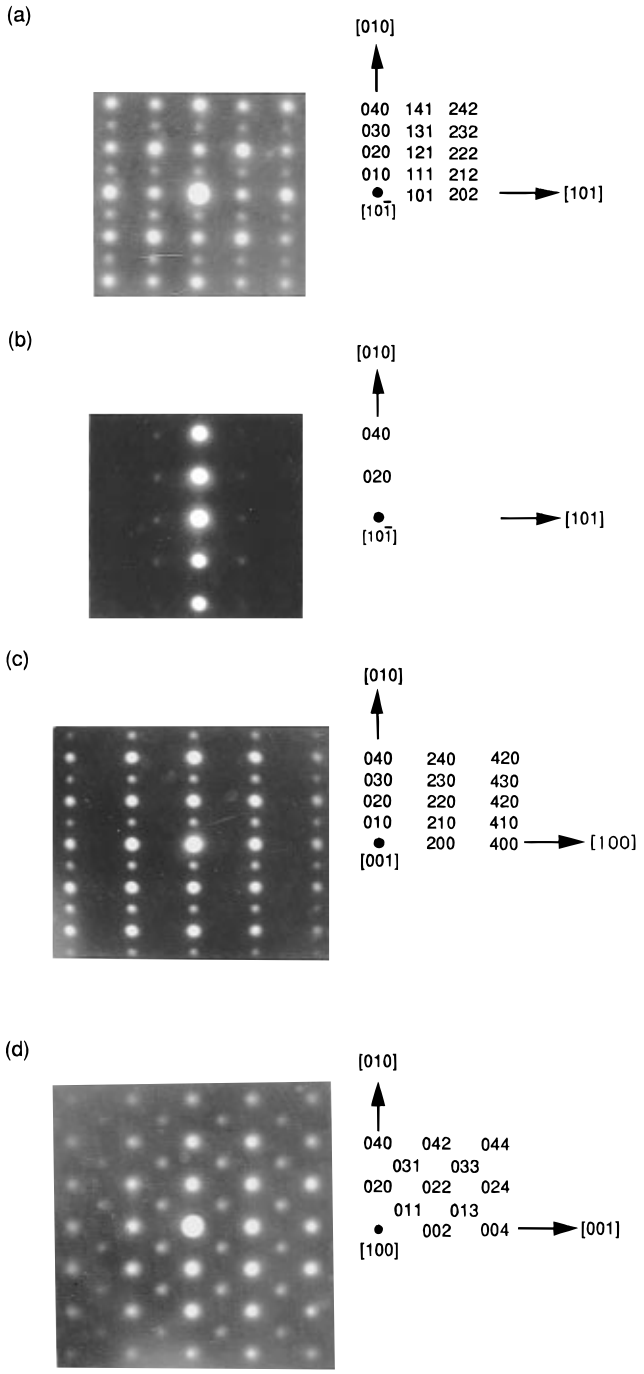

Figure 7. Electron diffraction patterns and corresponding peak indexes for the $La_{0.97}Ti_{0.8}V_{0.2}O_3$ phase. (a) The [$\bar{1}$01] zone axis. (b) The same zone axis after tilting about the [010] axis. The $(0k0)$ reflections with $k \neq 2n$ disappear upon tilting showing that the true reflection conditions are $k = 2n$. (c) The [001] zone axis showing the $(hk0)$, $h = 2n$ reflection conditions. The $(0k0)$ reflections, $k \neq 2n$ are due to double diffraction and disappear upon tilting. (d) The [100] zone axis showing the $0kl$, $k + l = 2n$ reflection conditions. Note that the $(0k0)$ reflections show no violations due to the inability to form double diffraction peaks in this zone axis.

(35) (a) Eitel, M.; Greedan, J. E. *J. Less-Common Met.* **1986**, *116*, 95. (b) Maclean, D. A.; Ng, H. K.; Greedan, J. E. *J. Solid State Chem.* **1979**, *30*, 35.

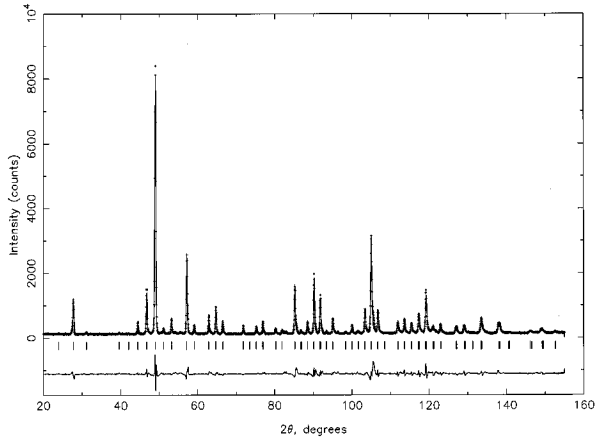

Figure 8. Calculated (continuous line) and observed (crosses) neutron diffraction profile of $La_{0.97}Ti_{0.8}V_{0.2}O_3$. A difference curve ($I_{obs} - I_{calc}$) is plotted at the bottom. Allowed reflection positions are noted by the vertical bars.

Table 2. Refined Structural Parameters[a] for $La_{0.97}Ti_{0.8}V_{0.2}O_3$ at 50 K

atom	site symmetry	*x*	*y*	*z*	*B*(iso)	frac
La	.*m*.	0.0344(5)	0.25	0.9944(10)	0.18(6)[b]	0.97(1)
Ti	1	0.5	0	0	0.18(6)[b]	0.82(1)[c]
V	1	0.5	0	0	0.18(6)[b]	0.18(1)[c]
O(1)	.*m*.	0.4886(8)	0.25	0.0771(11)	0.63(19)	1.09(4)
O(2)	1	0.2862(10)	0.0344(5)	0.7142(9)	0.77(12)	0.99(2)

[a] Space group = *Pnma* (62); $a = 5.57764(22)$, $b = 7.87738(32)$, $c = 5.57354(24)$, $R_p = 8.26$, $R_{wp} = 12.11$, $\chi^2 = 11.61$. [b] Constrained to be equivalent. [c] Constrained to sum to 1.

Table 3. Comparison of Structural Parameters of the $LaTi_{1-x}V_xO_3$ Phases

	multiplicity	$LaTiO_3$[b]	$La_{0.97}Ti_{0.8}V_{0.2}O_3$[c]	$LaVO_3$[d]
		Bonds[a]		
La−O(1)	1×	2.45(3)	2.438(9)	2.422(7)
La−O(1)	1×	3.05(1)	3.073(4)	3.036(3)
La−O(1)	1×	3.17(3)	3.160(9)	3.150(7)
La−O(1)	1×	2.60(1)	2.569(5)	2.580(4)
La−O(2)	2×	3.31(1)	3.291(8)	3.271(3)
La−O(2)	2×	2.77(1)	2.743(5)	2.780(3)
La−O(2)	2×	2.70(1)	2.701(5)	2.668(3)
La−O(2)	2×	2.47(1)	2.480(6)	2.450(4)
M−O(1)	2×	2.025(1)	2.009(2)	2.001(1)
M−O(2)	2×	2.033(1)	2.008(6)	2.003(4)
M−O(2)	2×	2.041(1)	2.012(6)	2.004(4)
M−O (ave)	6×	2.033	2.01	2.00
		Angles		
M−O(1)−M		154.53(7)	157.1(4)	157.054
M−O(2)−M		153.46(5)	157.48(25)	156.969
M−O−M (ave)		154.0	157.3	157.0
O(1)−M−O(1)		180.00	180.00	180.00
O(1)−M−O(2)		89.597	89.75(26)	89.840
		90.988	90.53(22)	90.840
		90.403	90.25(26)	90.263
		89.012	89.47(27)	89.160
cell	*a*	5.5844(1)	5.5776(2)	5.55548(4)
	b	7.9010(1)	7.8776(3)	7.84868(6)
	c	5.6301(1)	5.5735(3)	5.55349(5)

[a] M = Ti or V. [b] Data from ref 35a, powder neutron refinement, 10 K. [c] This work, powder neutron refinement, 50 K. [d] Data from ref 34, powder neutron refinement, 298 K. The metric parameters of the lower temperature structure (150 K) were not appreciably different.

t_{2g} π^* bands[36] that split into the upper and lower Hubbard bands in the $d^1 \rightarrow d^2$ systems.

Transport Properties. The resistivities (ρ) of the $LaTi_{1-x}V_xO_3$ samples (arc-melted pellets) with $0 \leq x \leq 0.5$ were measured between 300 and 4 K, and the results

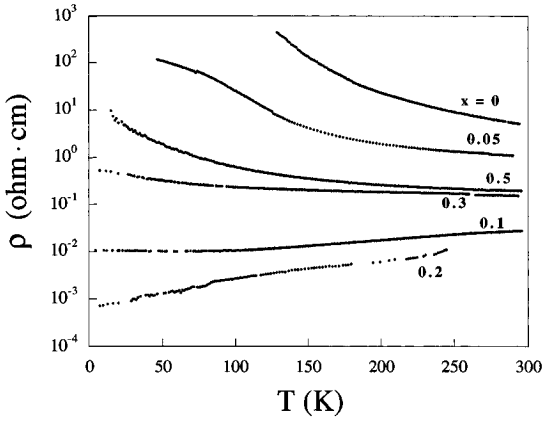

Figure 9. Plots of resistivity versus temperature for representative $LaTi_{1-x}V_xO_3$ phases.

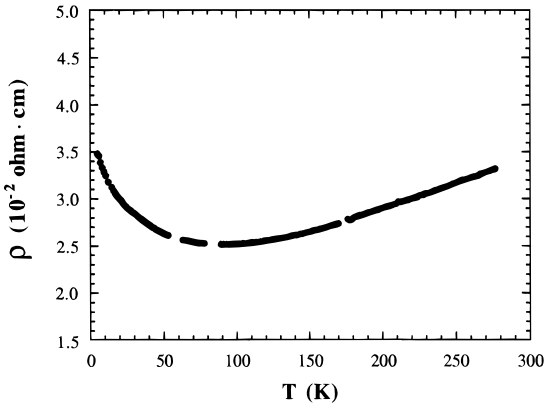

Figure 10. Plot of resistivity versus temperature for $La_{0.97}Ti_{0.75}V_{0.25}O_3$.

are shown in Figure 9. In agreement with previous studies,[23−25] $LaTiO_3$ shows semiconducting behavior with a room temperature resistivity of approximately 8 Ω cm. The substitution of V^{3+} for Ti^{3+} causes a decrease in resistivity and, at $x = 0.10$, metallic behavior is initiated. Compounds in the $0.10 \leq x \leq 0.25$ region exhibit metallic temperature dependencies with rather large resistivities at all temperatures (room temperature resistivities of $\sim 10^{-2}$ Ω cm). For $x > 0.25$, semiconducting behavior is observed with resistivities increasing with increasing V^{3+} concentration. Metallic samples containing microscopic cracks in the cut blocks showed flattened temperature dependencies relative to those data shown in Figure 9. Hysteresis was not observed in any of the samples measured.

The resistivities of some of the metallic phases show upturns at low temperatures that may be due to grain boundary effects (see Figure 10 for example). Unlike the related $R_{1-x}A_xTiO_3$ phases (R = La, Nd; A = Ca, Sr, Ba),[12,13,18] the upturns do not appear to be associated with any magnetic ordering and may be associated with electron localization due to impurity scattering.

Magnetic Properties. The magnetic susceptibilities (χ) of the $LaTi_{1-x}V_xO_3$ samples were measured between 4 and 300 K at an applied field of 1 kG. The data are summarized in Table 1. The susceptibility of oxygen precise $LaTiO_{3.00}$ shows an onset of magnetic ordering at ~140 K (Figure 11) which is in excellent agreement with the reported canted antiferromagnetism of the

(36) Greedan, J. E. *J. Less-Common Met.* **1985**, *111*, 335.

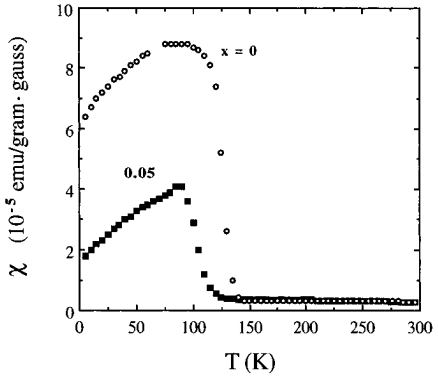

Figure 11. Plots of magnetic susceptibility versus temperature for $LaTiO_3$ and $LaTi_{0.95}V_{0.05}O_3$.

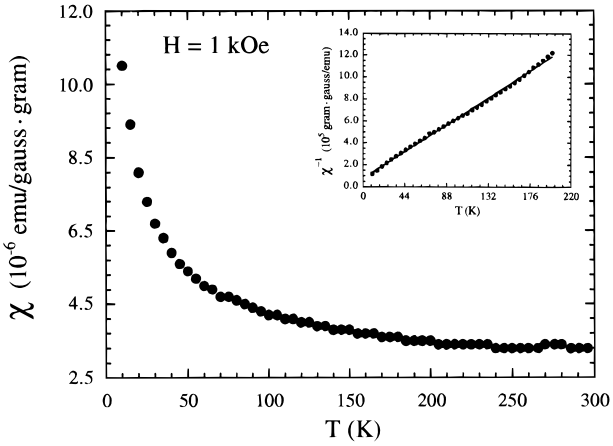

Figure 12. Plot of magnetic susceptibility versus temperature for $La_{0.97}Ti_{0.80}V_{0.20}O_3$. The inset shows the inverse susceptibility versus temperature.

compound where $T_N = 148$ K.[23] Substitution of V^{3+} lowers the ordering temperature to 120 K for the $x = 0.05$ sample and quenches the antiferromagnetic ordering completely by $x = 0.10$. The $LaTi_{1-x}V_xO_3$ phases in the composition range $0.1 \leq x < 0.3$ show large temperature-independent paramagnetism (TIP) and Curie−Weiss behavior below 200 K. The susceptibility of $La_{0.97}Ti_{0.8}V_{0.2}O_3$ is shown in Figure 12 as an example. The temperature-independent terms (χ_0) obtained from the Curie−Weiss fittings were 1.3×10^{-3} emu/mol for the $x = 0.1$ and 6.3×10^{-4} emu/mol for the $x = 0.2$ samples. These TIPs are proportionally larger than those observed in the metallic $R_{1-x}Ba_xTiO_3$ phases, which have less than one electron per formula unit. Using the assumption that spin $^1/_2$ ions are the sources of the Curie−Weiss behavior, the number of paramagnetic carriers of the $x = 0.1$ and 0.2 samples were estimated from the corresponding Curie constants (C). Multiple measurements on various samples consistently gave $S = {}^1/_2$ concentrations of approximately 10% for both compositions (~2.5% for an $S = 1$ model) suggesting that the moments may be intrinsic and not due to ferromagnetic impurities.

The magnetic susceptibilities of the $LaTi_{1-x}V_xO_3$ samples for $x \geq 0.3$ show TIP behavior as well with unusual peaks that move to higher temperatures as the V^{3+} concentration increases (Figure 13). For example, the magnetic susceptibilities of the $x = 0.3$, 0.5, and 0.7 samples show peaks at 10, ~14, and ~25 K, respectively (see Figure 14).

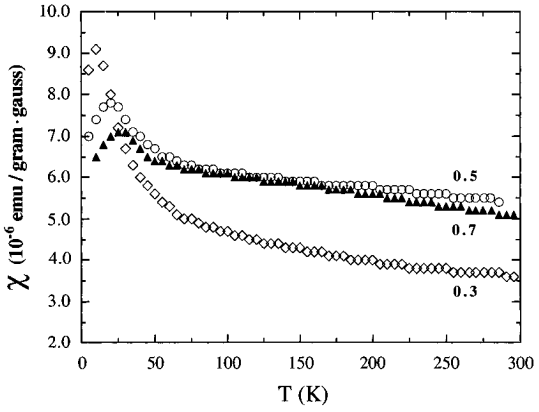

Figure 13. Plots of magnetic susceptibility versus temperature for the $LaTi_{1-x}V_xO_3$ samples where $x = 0.3$, 0.5, and 0.7.

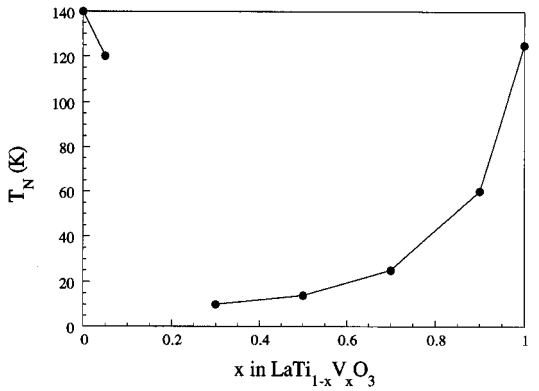

Figure 14. Plot of the magnetic susceptibility "peak" temperatures (T_N) versus x for the $LaTi_{1-x}V_xO_3$ samples.

The magnetic susceptibilities of the $LaTi_{0.1}V_{0.9}O_3$ ($x = 0.9$) and $LaVO_3$ ($x = 1.0$) samples depend on cooling conditions (see Figures 15 and 16). When the samples are cooled in the absence of field (zero field cooled, ZFC), the susceptibilities show only slight temperature dependencies upon warming. In contrast, the magnetic susceptibilities show peaks when the samples are field cooled (FC). The FC peak in the $LaTi_{0.1}V_{0.9}O_3$ sample appears at ~60 K (Figure 15), which is higher than that of the $x = 0.5$ and 0.7 samples (see Figure 13). The FC $LaVO_3$ sample shows a peak at ~135 K and a large diamagnetism below 125 K (Figure 16) consistent with the findings of Mahajan et al.[28] The magnitude of this diamagnetism is on the order of −3 emu/mol.

Discussion

Although it has been well-known that the $LaMO_3$ phases where M = Ti, V are distorted perovskites, there has been a large degree of controversy concerning the exact crystal symmetry of each. For example, $LaVO_3$ has been characterized as a cubic perovskite,[27] a tetragonally distorted perovskite,[28,37] and a hexagonally distorted perovskite[38] to name a few. The room-temperature orthorhombic $GdFeO_3$-type structure (space group *Pnma*) of $LaVO_3$ was recently assigned from synchrotron X-ray diffraction and neutron diffraction studies.[34] A similar controversy was found for $LaTiO_3$.[35,39−42] It is now generally accepted that both

(37) Kestigian, M.; Dickinson, J. G.; Ward, R. *J. Am. Chem. Soc.* **1957**, *79*, 5598.
(38) Dougier, P.; Casalot, A. *J. Solid State Chem.* **1970**, *2*, 396.
(39) Kestigian, M.; Ward, R. *J. Am. Chem. Soc.* **1954**, *76*, 6027.

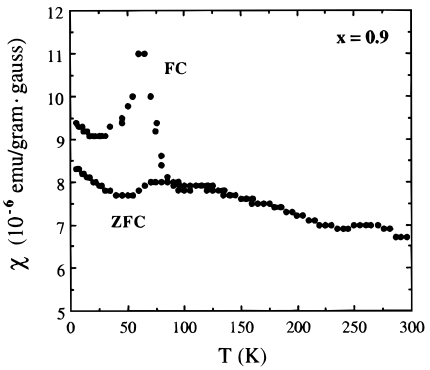

Figure 15. Plots of field-cooled (FC) and zero-field-cooled (ZFC) magnetic susceptibilities versus temperature for $LaTi_{0.90}V_{0.10}O_{3.0}$.

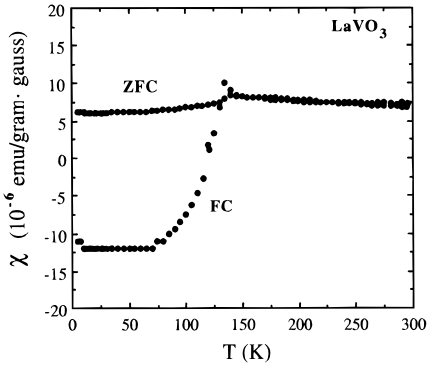

Figure 16. Plots of field-cooled (FC) and zero-field-cooled (ZFC) magnetic susceptibilities versus temperature for $LaVO_{3.0}$.

$LaTiO_3$ and $LaVO_3$ adopt orthorhombic perovskite $GdFeO_3$-type structures with *Pnma* crystal symmetry.[34,36] Despite the discrepancies in the assigned crystal structures, it is agreed that $LaVO_3$ is a semiconductor with an activation energy of ~0.14 eV.[28] The magnetic susceptibility shows a maximum at ~140 K which was attributed to antiferromagnetic ordering.[10,26−28] It is also now established that $LaTiO_{3.00}$ is an antiferromagnetic insulator with a T_N = 148 K and a bandgap of ~0.01 eV.[23−25]

The properties of the "$LaTiO_{3+\delta}$" phases are very sensitive to the oxygen stoichiometry. Lichtenberg et al.[23] reported that metallic conductivity is obtained when $\delta > 0.07$. Recent studies by Greedan and coworkers[24,25] have shown that these "oxygen excess" phases where $0 < \delta \leq 0.20$ are actually La-deficient compounds of formula $La_{1-x}TiO_3$ where $0 \leq x \leq 0.33$. Accordingly, the homogeneities and the oxygen contents of the $LaTi_{1-x}V_xO_3$ samples were closely monitored to probe for metallic $La_{1-x}TiO_3$ contaminants. The EDX analysis and TGA results indicate that the metallic behavior in the composition range $0.15 \leq x < 0.25$ is not due to excess oxygen. In fact, attempts to introduce excess oxygen into these compounds result in heterogeneous samples in which the impurity phases were clearly identifiable (e.g., $LaVO_4$, La_2O_3). Likewise, compositions with excessive lanthanum deficiencies (>5%) give multiphase products.

It is not obvious why solid solutions of two antiferromagnetic insulators would give metallic phases. This is especially surprising for *B*-site-substituted transition-metal oxide systems. Formation of solid solutions through disordered substitutions on perovskite *B* sites in metallic ABO_3 phases (B = transition metal) invariably localizes electrons and results in insulating behavior. For example, the substitution of Ru by Fe or Ga in the metallic $LaRuO_3$ phase ($LaRu_{1-x}B_xO_3$, B = Fe, Ga)[43,44] introduces impurities directly into the conduction band, causing localization of electrons. Similar affects were observed in the $LaNi_{1-x}B_xO_3$ (B = Cr, Mn, Fe) series in which metallic conductivity of $LaNiO_3$ is destroyed by very low-level chemical substitutions on the Ni sites.[45] Metallic $BaVS_3$ is also driven to an insulating state by Ti^{4+} substitution for V^{4+} in the $BaV_{1-x}Ti_xS_3$ system.[46] The substitution of Ti^{3+} (≤20%) for V^{3+} in the insulating $LiVO_2$ phase, which has a ordered rock salt structure with short V−V contacts, does not result in the delocalization of electrons and the compounds within the solid solutions remain insulating.[47] The presence of metallic-like conductivity in the $LaTi_{1-x}V_xO_3$ is more akin to the M−I transitions observed in the $BaPb_{1-x}BO_3$ solid solutions (B = Bi, Sb) that contain the superconducting compounds $BaPb_{0.70}Bi_{0.30}O_3$ (T_c = 13 K)[48] and $BaPb_{0.75}Sb_{0.25}O_3$ (T_c = 3.5 K)[49] at the M−I boundaries.

For the few *B*-site-substituted compounds that show metallic conductivity or superconductivity, the metal oxide sublattices are ordered with different *B*-site ions partitioned into separate layers. The conducting layer must be "uncontaminated". A classic example of this phenomenon is the superconducting $Y_{1-x}Ca_xSr_2Cu_2GaO_7$ systems,[50] where $^2_\infty[CuO_{4/2}]$ and $^2_\infty[GaO_{4/4}]$ layers are completely segregated. In structurally related copper oxides where substitution for copper occurs in the $^2_\infty[CuO_{4/2}]$ planes in a disordered fashion, intrinsic semiconductors are obtained at very low levels of substitution.[51,52] Although partial and complete ordering in related perovskite compounds has been well established (e.g., Sr_2PbSnO_4[53] and La_2CuSnO_6[54,55]), the electron, neutron, and synchrotron X-ray diffraction studies on $La_{0.97}Ti_{0.8}V_{0.2}O_3$ rule out ordering in the present compounds.

The origin of the metallic behavior in $LaTi_{1-x}V_xO_3$ is not obvious, and without further experiments, we can only speculate as to its source. For example, it is not clear to what extent (if any) the slight La nonstoichi-

(40) Bertaut, E. F. *J. Phys. Radium* **1956**, *17*, 129.
(41) Holzapfel, H.; Sieler, J. *Z. Anorg. Allg. Chem.* **1966**, *343*, 174.
(42) Ganguly, P.; Parkash, O.; Rao, C. N. R. *Phys. Status Solidi A* **1976**, *36*, 669.
(43) Bouchard, R. J.; Weiher, J. F.; Gillson, J. L. *J. Solid State Chem.* **1973**, *6*, 519.
(44) Bouchard, R. J.; Weiher, J. F.; Gillson, J. L. *J. Solid State Chem.* **1977**, *21*, 135.
(45) Rao, C. N. R. *Annu. Rev. Phys. Chem.* **1989**, *40*, 291.
(46) Matsuura, K.; Wada, T.; Nakamizo, T.; Yamauchi, H.; Tanaka, S. *Phys. Rev. B* **1991**, *43*, 13118.
(47) Goodenough, J. B.; Dutta, G.; Manthiram, A. *Phys. Rev. B* **1991**, *43*, 10170.
(48) Sleight, A. W.; Gillson, J. L.; Bierstedt, P. E. *Solid State Commun.* **1975**, *17*, 27.
(49) Tomeno, I.; Ando, K. *Phys. Rev. B* **1989**, *40*, 2690.
(50) Vaughey, J. T.; Thiel, J. P.; Hasty, E. F.; Groenke, D. A.; Stern, C. L.; Poeppelmeier, K. R.; Dabrowski, B.; Hinks, D. G.; Mitchell, A. W. *Chem. Mater.* **1991**, *3*, 935.
(51) Clayhold, J.; Ong, N. P.; Wang, Z. Z.; Tarascon, J. M.; Barboux, P. *Phys. Rev. B* **1989**, *39*, 7324.
(52) Chien, T. R.; Wang, Z. Z.; Ong, N. P. *Phys. Rev. Lett.* **1991**, *67*, 2088.
(53) Chen, B.-H.; Eichhorn, B. W. *J. Solid State Chem.* **1992**, *97*, 340.
(54) Anderson, M. T.; Poeppelmeier, K. R. *Chem. Mater.* **1991**, *3*, 476.
(55) Anderson, M. T.; Poeppelmeier, K. R.; Gramsch, S. A.; Burdett, J. K. *J. Solid State Chem.* **1993**, *102*, 164.

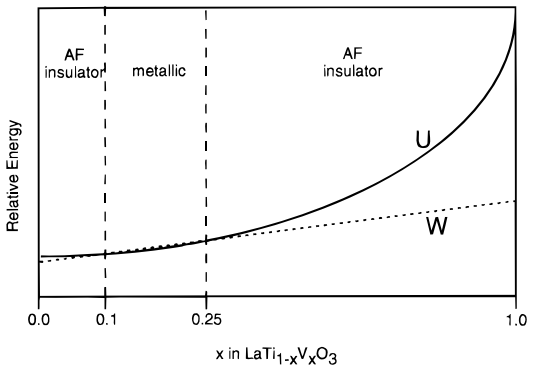

Figure 17. Proposed variation of the band widths (W) of the upper and lower Hubbard bands and the on-site Coulombic repulsions (U) for the $LaTi_{1-x}V_xO_3$ phases.

ometry plays in the transport properties. With this limitation in mind, we propose the following scenario. In $LaTiO_3$, it is clear that $U \approx W$ and a small widening of the Hubbard bands would produce $U/W \leq 1$, thus initiating metallic behavior. For $LaVO_3$, the Hubbard bands are presumably *somewhat* wider due to the small but distinct 0.03 Å contraction of the M−O bond distances and the 3° widening of the M−O−M angles. One can infer that the electron correlation is greater in $LaVO_3$ than in $LaTiO_3$ in that the bandgap (E_g) is larger for $LaVO_3$ (U/W for $LaVO_3 > U/W$ for $LaTiO_3$) despite the widening of the Hubbard bands. If one assumes that the change in W increases slightly with x, which is supported by the structural data, then the change in U in the $LaTi_{1-x}V_xO_3$ system must be nonlinear and "flat" at low values of x. A graphical representation of these proposed changes is shown in Figure 17. In the region where W rises above U, metallic behavior is observed, but as the electron correlations increase with increasing V^{3+} concentration, U again rises above W and AF insulators are again observed. The apparent nonuniform changes in structural parameters (i.e., $La_{0.97}Ti_{0.8}V_{0.2}O_3$ is structurally more similar to $LaVO_3$ than $LaTiO_3$, Table 3) would enhance this crossing of U and W at low values of x. Of course, Anderson localization may also become important as the vanadium concentration increases and may induce the onset of semiconducting behavior for $x > 0.25$.

The observed Pauli-type paramagnetism and metallic-like conductivity in the $LaTi_{1-x}V_xO_3$ samples is consistent with the findings in the $La_{1-x}A_xTiO_3$ (A = Sr, Ba) system[12,14,15,17] in that antiferromagnetic ordering and metallic conductivity do not coexist and the disruption of magnetic ordering is necessary to obtain the metallic conductivity. Similarly, the $Sr_{1-x}R_xVO_3$ phases (R = rare earth) show metallic behavior and large TIPs in the $0 \leq x \leq \sim 0.75$ range but are AF insulators for $x > 0.8$.[19] Although the $Sr_{1-x}R_xVO_3$ perovskites are isoelectronic with the $LaTi_{1-x}V_xO_3$ phases described here ($d^1 \rightarrow d^2$), the nature of the "doping" is obviously quite different.

The $LaTi_{1-x}V_xO_3$ phases exhibit complex magnetic properties whose interpretation is complicated by the presence of magnetic Ti^{3+} and V^{3+} ions on the B sites. The $LaTi_{1-x}V_xO_3$ phases where $0 \leq x < 0.1$ order as canted antiferromagnets with large TIPs above the ordering temperatures. Similar TIPs are observed in $RTiO_3$ phases where R = rare earth and yttrium.[56] It is currently not known what contributes to the large TIP in these materials although NMR studies on the related $La_{1-x}Sr_xVO_3$ system showed large Van Vleck contributions.

The insulating $LaTi_{1-x}V_xO_3$ samples with $x > 0.3$ show magnetic ordering with an increase of the ordering temperature as a function of V^{3+} concentration (see Figure 14); however, the type of magnetic ordering could not be determined from the existing data. We attribute the ordering to antiferromagnetic coupling based on the previous assignments in the $LaVO_3$ system,[28] although determination of the exact nature of the magnetism requires further experiments. $LaVO_3$ has a large diamagnetism that is $\sim 10^2$ times larger than the core diamagnetism. The appearance of this large diamagnetism in the field-cooled measurements rather than zero-field-cooled measurements and the absence of any transition to zero resistance in resistivity measurements[28] rule out superconductivity in this sample. Similar results have also been reported by Mahajan et al.[28] and Shirakawa et al.[57] as well. The source of this diamagnetism is currently not known.

In summary, a series of compounds with the general formula $LaTi_{1-x}V_xO_3$ have been prepared and shown to adopt $GdFeO_3$-type structures. The $LaTi_{1-x}V_xO_3$ phases display unusual physical properties in that metallic-like behavior is obtained from the solid solutions of antiferromagnetic Mott−Hubbard insulators $LaTiO_3$ and $LaVO_3$. The initiation of metallic behavior upon disordered B-site substitution is quite rare.

Acknowledgment. This work was funded by the NSF-DMR (9223060) and Electric Power Research Institute. The work at Brookhaven National Laboratory was performed under contract DE-AC02-76CH00016, U.S. Department of Energy, Division of Materials Sciences and Division of Chemical Sciences.

CM950351Q

(56) Maclean, D. A.; Greedan, J. E. *Inorg. Chem.* **1981**, *20*, 1025.
(57) Shirakawa, N.; Ishikawa, M. *Jpn. J. Appl. Phys.* **1991**, *30*, 755.